A New Control Technique for Regulating the Synchronous Generator Frequency Based on OFSTPID

Abdel Azim Salem[1], Shorouk Osama[2], M.Abdelghany[3], Amgad Salem[4]

[1,2,3,4] Faculty of Engineering, Electrical Engineering Dept., October 6 University
[1]abdelazim.salem.eng@o6u.edu.eg
[2]shorouk.eng@o6u.edu.eg
[3]m.a.abdelghany.eng@o6u.edu.eg
[4]amgadaboraya.eng@o6u.edu.eg

.

Abstract – *This paper addressed the analysis, and control for tracking the active power flow (APF) from the synchronous generator (SG). The proposed control relies on the real concept of interaction between (active/reactive) and (governor/exciter voltage). The proposed system is tested by disturbance in active load by increasing or decreasing in 0.1pu. To address this disturbance, traditional controllers such as PID may not suffice for optimal performance. Thus, the Self-Tuning Controller (FST) emerges as a promising solution for PID controllers. Utilizing an Ant Colony Optimization (ACO), PID parameters can be effectively tuned. As a result, two control units of the Self-Tuning PID Controller (OFSTPID) are employed for active and reactive power control loops. This approach enhances active Power Filter (APF) satisfaction while meeting the constant demand for reactive power, thereby enhancing the reliability and quality of the power system. Comparative analysis against relevant literature demonstrates that this methodology leads to improved load frequency Control (LFC) performance and effective compensation for reactive power.*

Keywords*: Turbo-generator, Active power flow, Reactive power flow, fuzzy self-tunning PID and infinite bus bar, Ant Colony Optimization.*

I. Introduction

The complexity of electrical power systems is steadily increasing due to factors such as the rise in renewable energy sources, load forecasting, reliability and security concerns, large data volume exchanges, and power quality issues [1]. These factors directly impact the stability, operation, and security of power system networks. Power quality parameters, particularly voltage and frequency, are of utmost importance and have been a focus of research attention over the past two decades.
Fluctuations in load nature affect active and reactive power demands, leading to deviations in power system frequency and voltage levels, which can disrupt normal operation [2],[3]. Automatic Generation Control (AGC) or Load Frequency Control (LFC) and Automatic Voltage Regulator (AVR) systems are installed in generating stations to maintain nominal frequency and voltage values within acceptable standards during variations in power demands. The interconnected control loops of LFC and AVR play crucial roles in achieving this. While some researchers concentrate on decoupling LFC and AVR to facilitate active power demand control without considering voltage variation, others focus solely on AVR without addressing frequency variation [4]–[8]. However, in practical power systems, the interdependence between frequency and voltage cannot be overlooked [9]–[11]. With the increasing integration of renewable energy resources and fluctuating consumer demand, the uncertainty of active and reactive power in power systems has heightened. Consequently, frequency oscillations and variations in generator terminal voltage occur Thus, there is a need for more robust and reliable LFC and AVR methodologies to address these challenges. This paper proposes an LFC-based methodology that also considers the stability of generator terminal voltage control. By incorporating both aspects, the power system can maintain the nominal frequency while ensuring no disturbance in reactive power demands or synchronous generator terminal voltage.
The primary challenge in electrical power system operation is maintaining real-time control over generator frequency and terminal voltage. Deviations in these parameters can severely impact the performance of interconnected equipment [12]- [13]. Control mechanisms like Load Frequency Control (LFC) and Automatic Voltage Regulation (AVR) are crucial for stabilizing frequency and voltage within desired limits. LFC reduces the gap between power demand and generated power, regulating frequency, while AVR does the same for voltage [14]- [15]. Recently, researchers have explored combining LFC and AVR techniques, utilizing various control strategies such as fuzzy logic

control (FLC) and PID controllers. These combined systems have been applied to different power generation setups, including solar thermal and hydrothermal units, employing optimization algorithms like simulated annealing (SA) and moth flame optimizer (MFO) [16]. In more complex systems, such as multi-area setups, advanced controllers like Integral-double derivative controller with derivative [16]. In [13], [17] filter (IDDF) and techniques like lightning search algorithms (LSA) have been used. Due to the intricate nature of system dynamics, traditional controllers struggle to handle large disturbances effectively, necessitating the use of optimized methods like FSTPID.

Authors have considered a single-machine infinite bus reality power system, as illustrated in Fig. 1. Generally, the reality power system consists of outer loop and inner loop control. The outer loop is for governor position control, and the inner loop is for field voltage control. There is a tight relationship between the two inner/outer control loops represented by four gains G1, G2, G3, and G4. The evaluation of these gains will be discussed in Section III.

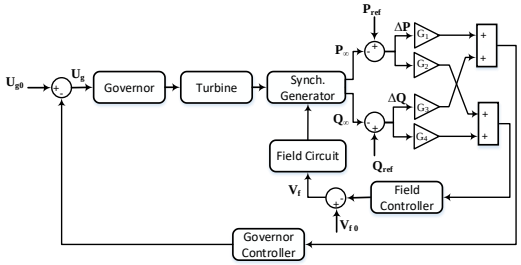

Fig.1 Reality power system control scheme

The TGS with steam valve control is the main component of the system. It can be described as shown in Fig.2. The TGS is connected to infinite bus through step up transformer and two parallel transmission lines as shown in Fig.2. The steam turbine contains three stages which are the high-pressure turbine (HPT), intermediate-pressure turbine (IPT), and low-pressure turbine (LPT). The steam flow is controlled by the governor position (U_g) while, the induced generator voltage internal is controlled by exciter field voltage (E_f). The grid or infinite bus is supplied with active power (P_∞) and reactive power (Q_∞) by the generator. The voltage and frequency at the infinite bus are constant.

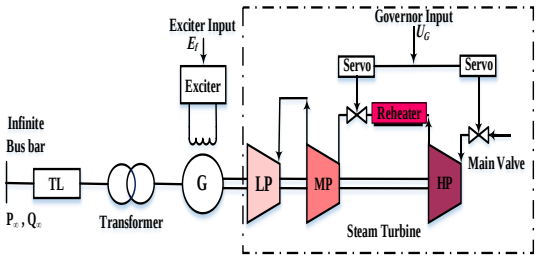

Fig.2 Turbo-Generator system connected to infinite bus.

This paper adopts the OFSTPID for the TGS. The method relies on parameter adjustment of PID gains using optimization as the first step, followed by designing FLC gains using membership functions and fuzzy rules as the second step [18]. The adaptation output parameters of OFSTPID are determined by multiplying the output gains of PID and FLC. Thus, the output control action of the OFSTPID controller depends on the algorithm of PID parameter selection and the design of fuzzy rules and scaling factors. OFSTPID offers several advantages over traditional controllers, including covering a wider range of operating conditions, being cheaper to develop, and automatically improving an initial approximate set of fuzzy rules. Additionally, optimal design parameters are determined by the ACO method. In this paper, the following contributions are made:

- Designing a TAPF model for TGS to control generating station frequency and terminal voltage.
- Implementing intelligent-based OFSTPID as a controller for each active power and reactive power loop.
- Utilizing ACO for tuning control parameters.
- Demonstrating the superiority of OFSTPID over conventional PID controls.
- Justifying and demonstrating the coupling of LFC with AVR using mathematical analysis.
- Comparing and assessing the performance of the proposed system against different control methods.

The paper is organized as follows: Section II defines the problem, section III presents the modeling and analysis of the reality system, section IV presents the proposed system parameters optimization, section V discusses the results to verify the proposed control scheme, and finally, the conclusions are listed in section VI

II. Problem definition

In various studies ([4], [5], [20), authors have proposed diverse methodologies for implementing the Load Frequency Control (LFC) strategy in power systems. Their findings confirmed improvements in active power and frequency. However, a significant decline in system response, particularly in reactive power generation, was observed, as depicted in Fig. 3, which will be elaborated upon. In Fig. 3a, the authors suggested that the LFC system remains stable when employing a PID controller at a specific operating point of 0.8pu of active power demand at the infinite bus bar (Pref) during the period from 0 to 5 seconds. System requirements were adjusted by ±10%pu, resulting in reaching 0.88pu/0.72pu from 5 to 20 seconds and from 35 to 50 seconds, respectively. Pref was restored to the operating point (0.8pu) during the intervals 20 to 35 seconds and 50 to 70 seconds. In the proposed system, the ±10%pu variation in active load represents a significant disturbance compared to other studies where load variation ranged from 0.01pu to 0.06pu [7], [19]– [22]. The conventional LFC control technique involves regulating the governor position solely to control the Active Power Flow (APF), while the exciter field voltage

remains constant because Reactive Power Flow (RPF) does not change. Consequently, the APF response at the infinite bus (Pꝏ) has been adjusted to match the desired value, as depicted in Fig. 3b. Fig. 3c illustrates the steady-state value of the governor position response, which has increased or decreased by ±10.1%. The response of the governor valve position (Ug) is directly proportional to Pꝏ. Variations in the governor position have led to an increase in the power angle (δ) to 53.20 (14.1%) and a decrease to 40.750 (12.6%), as depicted in Fig. 3d. Fig. 3e displays the frequency deviation (Δf) during load variation, with the overshoot value reaching ±0.0075 Hz (0.00015pu), while the steady-state response tends toward zero.

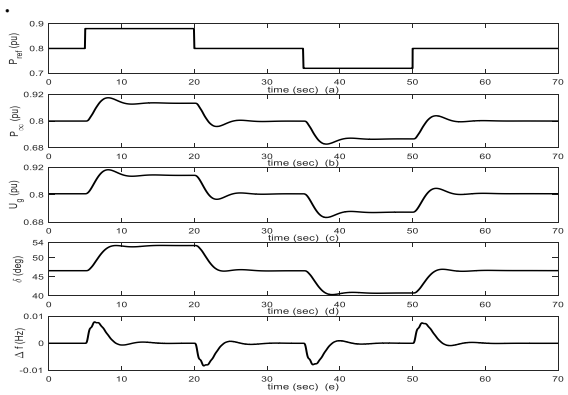

Fig.3 APF and related response of the conventional LFC for PID controller. a-Active power demand reference; -b- APF response at the infinite bus bar (P_{∞}); c- Governor position response (U_g); d- Power angle response (δ); e- Change in the frequency response (Δf).

Fig. 4a illustrates the adjustment of the reactive load demand (Qref) at a constant operating point (0.6pu) throughout the simulation period from 0 to 70 seconds. Fig. 4b depicts the Reactive Power Factor (RPF) at the infinite bus (Qꝏ). Although the actual value of Qꝏ did not meet the set point, the response was significant. The RPF decreased to 0.525pu (12.5%) between 5 and 20 seconds, while the Active Power Factor (APF) in Fig. 3b increased by 10%. Between 35 and 50 seconds, the RPF increased to 0.66pu (10%), while the APF in Fig. 3b decreased by 10%. The adverse effects of the reverse action response of RPF with APF lead to a decrease in power quality and reliability of the power system [23]. Fig. 4c demonstrates the constancy of the field excitation voltage response (Ef) at 2.659pu throughout the simulation, corresponding to the concept of Load Frequency Control (LFC). Generally, the terminal generator voltage response (Vter) in Fig. 4d is directly proportional to Qꝏ. Therefore, the value of Vter decreased by 2.1% between 5 and 20 seconds while Qꝏ decreased by 12.5%, and the value of Vter increased by 1.7% between 35 and 50 seconds while Qꝏ increased by 10%.

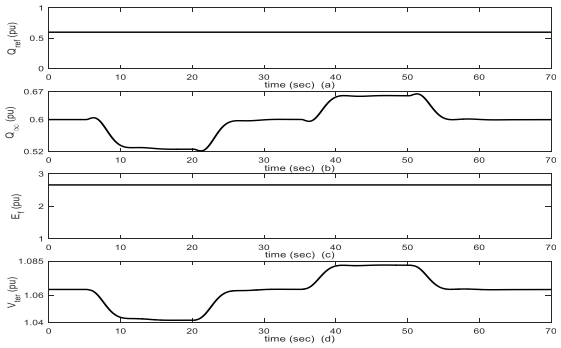

Fig.4 RPF and related response of the conventional LFC for PID controller. a-Reactive power demand reference; -b- RPF response at the infinite bus bar (Q_{∞}); c- Exciter field voltage response (E_f); d- Generator terminal voltage response (V_{ter}).

III. Proposal of Modeling and analysis of reality power system

In Section II, simulation results indicate a discrepancy in the relationship between APF and RPF of the turbo-generator. To address this, the authors will employ analytical concepts from power systems to develop a mathematical formulation ensuring the fulfillment of both active and reactive power demands incrementally. The power system depicted in Fig. 1 can be simulated under steady-state conditions as a synchronous generator. This generator comprises a back-induced electromotive force (Eg) and synchronous impedance, interconnected with other network equivalent circuits. The equivalent circuits representing the infinite bus bar denote a constant voltage source, designated as a voltage reference (Vꝏ). Thus, the power system's reality can be modeled as a two-port network, as illustrated in Fig. 5. Here, A and B represent constants associated with the system configuration, the acquisition of which will be discussed in this section.

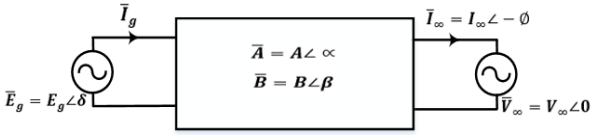

Fig.5 Two-port network system

The mathematical model of the reality power system consists of two proposal models where that each model complements the other. The first proposal considered extraction of new power equations using apply two-port network. The second proposal considered evaluation of the operators of G_1, G_2, G_3 and G_4 in Fig.1 to control the active and reactive power flow.

- The first proposal can be derived by the following equations,

$$\bar{E}_g = \bar{A}\bar{V}_\infty + \bar{B}\bar{I}_\infty \quad (1)$$

$$\bar{I}_\infty = \frac{\bar{E}_g}{\bar{B}} - \frac{\bar{A}}{\bar{B}}\bar{V}_\infty \quad (2)$$

$$\bar{I}^*_\infty = \frac{\bar{E}^*_g}{\bar{B}^*} - \frac{\bar{A}^*}{\bar{B}^*}\bar{V}^*_\infty \quad (3)$$

But,

$$\bar{S}_\infty = P_\infty + jQ_\infty = \bar{V}_\infty\bar{I}^*_\infty \quad (4)$$

$$\bar{S}_\infty = \frac{\bar{E}^*_g}{\bar{B}^*}\bar{V}_\infty - \frac{\bar{A}^*}{\bar{B}^*}V^2_\infty \quad (5)$$

So,

$$\bar{S}_\infty = \frac{E_g}{B}V_\infty\angle\beta-\delta \ -\frac{A}{B}V^2_\infty\angle\beta-\alpha \quad (6)$$

$$P_\infty = \frac{E_g}{B}V_\infty cos(\beta-\delta) \ -\frac{A}{B}V^2_\infty cos(\beta-\alpha) \quad (7)$$

$$Q_\infty = \frac{E_g}{B}V_\infty sin(\beta-\delta) \ -\frac{A}{B}V^2_\infty sin(\beta-\alpha) \quad (8)$$

For open circuit at infinite bus ($I_\infty = 0$);

$$\bar{A} = \frac{\bar{E}_g}{\bar{V}_\infty} \quad (9)$$

For short circuit at infinite bus ($V_\infty = 0$);

$$\bar{B} = \frac{\bar{E}_g}{\bar{I}_\infty} \quad (10)$$

According to network configuration, the operator values ofA and B are depended on the connection of the network components. To control the active and reactive power flow to the infinite bus, the values of power and generated voltage (E_g) must be controlled simultaneously referring to the equations (7), (8). But, the power angle and the generated voltage (E_g) can be regulated by the governor position (Ug) and the field exciter voltage (E_f) respectively. By applying the Taylor series in two variables on equations (7) and (8);

$$\Delta P_\infty = \frac{\partial P_\infty}{\partial E_g}\Delta E_g + \frac{\partial P_\infty}{\partial\delta}\Delta\delta \quad (11)$$

$$\Delta Q_\infty = \frac{\partial Q_\infty}{\partial E_g}\Delta E_g + \frac{\partial Q_\infty}{\partial\delta}\Delta\delta \quad (12)$$

By taking the partial derivative of equations(7) and (8);

$$\frac{\partial P_\infty}{\partial E_g} = \frac{V_\infty}{\beta}\cos(\beta-\delta) \quad (13)$$

$$\frac{\partial P_\infty}{\partial\delta} = \frac{E_g V_\infty}{\beta}\sin(\beta-\delta) \quad (14)$$

$$\frac{\partial Q_\infty}{\partial E_g} = \frac{V_\infty}{\beta}\sin(\beta-\delta) \quad (15)$$

$$\frac{\partial Q_\infty}{\partial\delta} = -\frac{E_g V_\infty}{\beta}\cos(\beta-\delta) \quad (16)$$

Knowing that, $\Delta P_\infty = P^N_\infty - P^O_\infty, \Delta Q_\infty = Q^N_\infty - Q^O_\infty, \Delta E_g = E^N_g - E^O_g$ and $\Delta\delta = \delta^N - \delta^O$

Where, P^N_∞ is the new active power at infinite bus,P^O_∞ is the old active power at infinite bus,Q^N_∞ is the new reactive power at infinite bus,Q^O_∞ is the old reactive power at infinite bus,E^N_g is the new voltage generation,E^O_g is the old voltage generation, δ^N is the new power angle andδ^O is the old power angle.

In equations (7) and (8), the maximum power is achieved if two conditions are achieved together; $(\delta = \beta), \cos(\beta-\delta) = 1$

The equation (7) can be reformulated as,

$$P^{max}_\infty = \frac{E_g V_\infty}{\beta} - \frac{\boldsymbol{A}}{\boldsymbol{B}}V^2_\infty cos(\beta-\alpha) \quad (17)$$

The first proposed analysis of relevant concept can be clarified as:

The angle β represents the phase angle of the total series impedance between the internal generated voltage E_g and the infinite bus voltage V_∞. The reactance of the total series impedance is greater than its resistance. So, at normal operation, $\delta < \beta$ and $45^0 < \beta < 90^0$.The trigonometric function of sin and cos is a positive sign If they are in the first quarter.So, $cos(\beta-\delta) = +ve$ value and $sin(\beta-\delta) = +ve$. That means that$\frac{\partial P_\infty}{\partial\delta} = +ve$ value,$\frac{\partial Q_\infty}{\partial E_g} = +ve$ value and $\frac{\partial Q_\infty}{\partial\delta} = -ve$ value**.** Based on these concept**s,** if $E_g$is constant value, $\delta$is varying due to variation in the active power (ΔP) and$P^N_\infty > P^O_\infty$, then $\Delta P = +ve$ value. This leads to $\delta^N > \delta^O$or$\Delta\delta = +ve$value. Then, the reactive power from equation (15) $\Delta Q = -ve$value. Also vice versa, if $\Delta P = -ve$ value, then $\Delta Q = +ve$ value. This explanation coincides the active and reactive power response in Fig. 3c and Fig. 3d.

- The second proposal of the factor estimation G_1, G_2, G_3 and G_4 can be deduced by the following equations,

From equation (11) and equation (12), The change in infinite bus active and reactive powers can be written as functions in the variation of generator internal voltage and the variation of the power angle as follows:

$$\Delta P_\infty = A_1\Delta E_g + B_1\Delta\delta \quad (18)$$

$$\Delta Q_\infty = A_2\Delta E_g + B_2\Delta\delta \quad (19)$$

where

$$A_1 = \frac{\partial P_\infty}{\partial E_g}, B_1 = \frac{\partial P_\infty}{\partial\delta}, A_2 = \frac{\partial Q_\infty}{\partial E_g} \ and \ B_2 = \frac{\partial Q_\infty}{\partial\delta}$$

The equations 18,19 can be reformed in the matrix form as follows:

$$\begin{bmatrix}\Delta P_\infty\\ \Delta Q_\infty\end{bmatrix} = \begin{bmatrix}A_1 & A_2\\ B_1 & B_2\end{bmatrix}\begin{bmatrix}\Delta E_g\\ \Delta\delta\end{bmatrix} \quad (20)$$

By inversing the matrix

$$\begin{bmatrix}\Delta E_g\\ \Delta\delta\end{bmatrix} = \frac{1}{A_1B_2-A_2B_1}\begin{bmatrix}B_2 & -A_2\\ -B_1 & A_1\end{bmatrix}\begin{bmatrix}\Delta P_\infty\\ \Delta Q_\infty\end{bmatrix} \quad (21)$$

$$\Delta E_g = \frac{1}{A_1B_2-A_2B_1}\ (B_2\Delta P_\infty - A_2\Delta Q_\infty) \quad (22)$$

$$\Delta E_g = G_1\Delta P_\infty + G_2\Delta Q_\infty) \quad (23)$$

Where;

$$G_1 = \frac{B_2}{A_1B_2 - A_2B_1}$$

$$G_2 = \frac{-A_2}{A_1B_2 - A_2B_1}$$

$$\Delta\delta = \frac{1}{A_1B_2 - A_2B_1}\ (-B_1\Delta P_\infty + A_1\,\Delta P_\infty) \quad (24)$$

$$\Delta\delta = G_3\,\Delta P_\infty + G_4\,\Delta Q_\infty) \quad (25)$$

Where;

$$G_3 = \frac{-B_1}{A_1B_2 - A_2B_1}$$

$$G_4 = \frac{A_1}{A_1B_2 - A_2B_1}$$

From the complete analysis of proposed mathematical model, the APF at infinite bus can be controlled by the input parameters of governor position (U_g) and field voltage (E_f) while maintaining the reactive power constancy ($Q_\infty^N = Q_\infty^O = const.$)

IV. Proposed of Reality System Parameters Optimization

The PID controller and FST together offer significant advantages in achieving optimal performance within power systems. Researchers have shown interest in utilizing the FSTPID controller to enhance response to voltage and frequency deviations in power systems [24], [25]. The OFSTPID controller structure comprises two main components:

A. Optimization of controller parameters for active and reactive power control loops:

This study focuses on optimizing the six parameters of the PID controller for both active power control loop (kp_P, ki_P, kd_P) and reactive power control loops (kp_Q, ki_Q, kd_Q) using the Ant Colony Optimization (ACO) method. ACO demonstrates effectiveness in providing solutions within short time frames, producing acceptable solutions through its greedy heuristic searching process, and avoiding premature convergence during distributed computation [26]– [28].

The Total Active Power Flow (TAPF) system is governed by the overall objective function (F_g), which can be expressed as:

$$F_g = F_1 + F_2 + F_3 + F_4 \quad (26)$$

The different objective functions$F_1, F_2, F_3 and\ F_4$are represented as:

1. Error minimization between desired and actual value of the active power demand over all the simulation time from 0:70 second. The integral square error (e_P) of active power loop is minimized by the form of equation (27).

$$F_1 = \int_0^t e_P^2(t)\,.\,dt \quad (27)$$

2. Improve the system performance of active power control loop which represents the rise time (t_{r_P}), over shoot (O_{s_P}), settling time (t_{s_P}) and steady state error (e_{ss_P}).The objective function in equation (28) represents the minimization parameters of t_{r_P}, O_{s_P}, t_{s_P} and e_{ss_P}.These parameters are weighted by scaling factors $\propto_P, \beta_P, \gamma_P and\ \delta_P$. The scaling factors are arbitrarily selected to enforce the priority of each individual objective

$$F_2 = \frac{1}{[\propto_P(t_{r\_P} - t_{r\_m\_p}) + \beta_P(O_{s\_P} - O_{s\_m\_p}) + \gamma_P(t_{s\_P} - t_{s\_m\_p}) + \delta_P(e_{ss\_P} - e_{ss\_m\_p})]} \quad (28)$$

Where $t_{r_m_p}, O_{s_m_p}, t_{s_m_p}\ and\ e_{ss_m_p}$are the rise time measurement, over shoot measurement, settling time measurement and steady state error measurement of the active power control loop respectively.

3. Error minimization between desired and actual value of the reactive power demand over all the simulation time from 0:70 second. The integral square error (e_Q) of reactive power loop is minimized by the form of equation (29).

$$F_3 = \int_0^t e_Q^2(t)\,.\,dt \quad (29)$$

4. Improve the system performance of reactive power control loop which represents the rise time (t_{r_Q}), over shoot (O_{s_Q}), settling time (t_{s_Q}) and steady state error (e_{ss_Q}).The objective function in equation (30) represents the minimization parameters of t_{r_Q}, O_{s_Q}, t_{s_Q} and e_{ss_Q}.These parameters are weighted by scaling factors $\propto_Q, \beta_Q, \gamma_Q and\ \delta_Q$. The scaling factors are arbitrarily selected to enforce the priority of each individual objective

$$F_4 = \frac{1}{[\propto_Q(t_{r\_Q} - t_{r\_m\_Q}) + \beta_Q(O_{s\_Q} - O_{s\_m\_Q}) + \gamma_Q(t_{s\_Q} - t_{s\_m\_Q}) + \delta_Q(e_{ss\_Q} - e_{ss\_m\_Q})]} \quad (30)$$

Where $t_{r_m_Q}, O_{s_m_Q}, t_{s_m_Q}\ and\ e_{ss_m_Q}$are the rise time measurement, over shoot measurement, settling time measurement and steady state error measurement of the reactive power control loop respectively.

The flowchart of ACO algorithm to determine the parameters' optimization process is illustrated in Fig. 6.

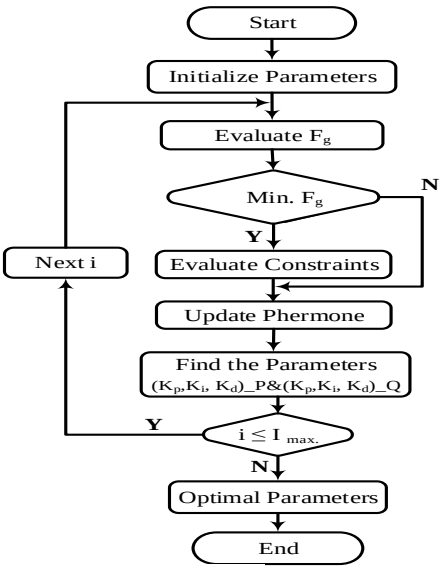

Fig. 6. Optimization process flowchart of ant colony algorithm.

B. Determination of control parameters based on fuzzy rules

The second part relies on updating the control response by using FSTPID controller to adjust the gains of (kp_P, ki_ P, kd_ P) and (kp_Q, ki_Q, kd_Q) to enhance the performance of reality power system against the

disturbance of the load variations. The FSTPID control system foreach one control loop is illustrated in Fig.7. the output of fuzzy controller is responsible for correcting the control action related to the error (e) and the change of error (Δe). The output of fuzzification process depend on membership structure of e, Δe and output as shown in Fig. (8) according to the rule base structure as illustrated in table 1. The defuzzification process is responsible to produce the gains ($K_{PF}, K_{IF} and K_{DF}$) by converting the fuzzy output to crisp values based on the center of gravity equation (31). The total output control action of FSTPID is represented by the equation (32).

$$u = \frac{\sum_{i=1}^{r} u(u_i)u_i}{\sum_{i=1}^{r} u(u_i)} (31)$$

Where $u(u_i)$ is the weight of membership the element (u_i) which is the output of the rule

$$U_{tun} = K_{P\_tun} + K_{I\_tun} \int edt + K_{D\_tun} \frac{de}{dt} \quad (32)$$

Where,$U_{tun}$is the total output control action of FSTPID, $K_{P\_tun} = K_P * K_{PF}$, $K_{I_{tun}} = K_I * K_{IF}$ and $K_{D\_tun} = K_D * K_{DF}$.

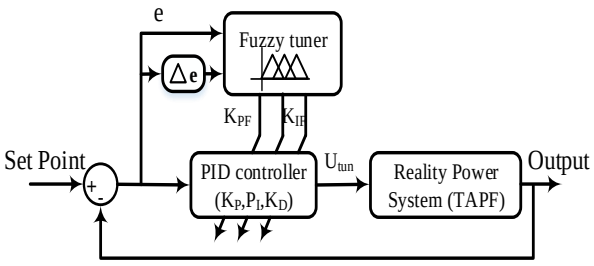

Fig. 7 Structure of FSTPID.

V. Results and Discussions

Authors employed two control techniques on the proposed system, illustrated in Fig. 1: the first being a PID controller and the second an OFSTPID controller. These were utilized to enhance the APF/RPF and associated output of the proposed system, depicted in Fig. 9 and Fig. 10. The active and reactive power demand, as shown in Fig. 3a and Fig. 4a, respectively, were applied to the proposed system. In Fig. 9a, the APF response accurately tracked the active power demand for each controller. Notably, during positive and negative load disturbances (5-20 seconds and 35-50 seconds), the response of the OFSTPID controller surpassed that of the PID controller. The PID controller's gain parameters were set as Kp=0.95, KI=1.27, and KD=0.0001. Throughout these load disturbances, the response of the OFSTPID controller stabilized before that of the PID controller. Fig. 9b depicts the governor valve position, exhibiting a nearly identical response for both controllers. In Fig. 9c, a critical observation distinguishes the proposed system from conventional LFC. Specifically, changes in the governor position caused the power angle to increase to 50.750 (8.88%) during positive load disturbance, whereas in conventional LFC (Fig. 3d), it increased to 53.2 (14.1%) in the same interval. Similarly, during negative load disturbance, the power angle decreased to 42.360 (9.1%) in the proposed system, compared to 40.750 (12.6%) in conventional LFC. The power angle difference between the two systems (2.450 during positive load disturbance and 1.60 during negative load disturbance) indicates a relative advantage of the proposed system in generating an APF to the electrical power system, surpassing conventional LFC at the same angle. Fig. 9d displays the frequency deviation of the OFSTPID controller, reaching zero before the PID controller, although with a higher peak overshoot during both positive and negative load disturbances. Notably, in Fig. 10, the response of the OFSTPID controller for the RPF and associated parameters (EF and Vter) outperforms that of the PID controller across all three figures (10a, 10b, and 10c).

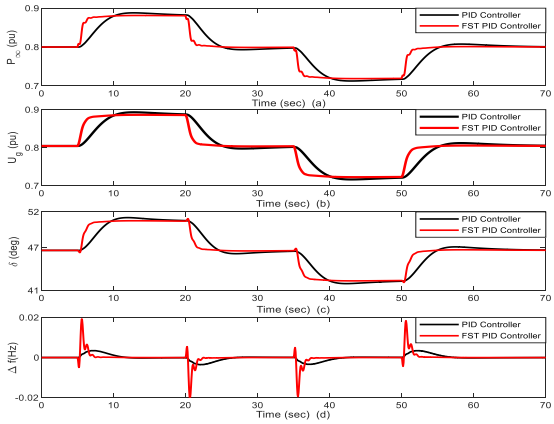

Fig.9 APF and related output response of the proposed methodology for PID and FSTPID controllers. a- P_{∞}; b- U_g; c- δ, d-Δf.

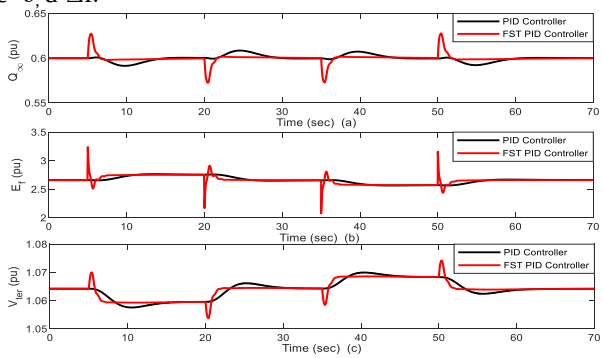

Fig.10 RPF and related output response of the proposed methodology for PID and FSTPID controllers. a- Q_{∞}; b- E_f; c- V_{ter}.

Table I demonstrates the disparities between recent research efforts and the proposed methodology concerning frequency deviation dynamic response. The comparison transparently outlines differences in settling time (Ts), peak overshoot (MP), peak time (Tp), and peak undershoot (UP) during positive active load disturbances within the interval of a positive load disturbance of 0.08pu. The comparative analysis establishes that the proposed method outperforms related research efforts in all dynamic parameters except settling time and peak

time as documented in reference [22]. However, it's worth noting that the settling time in the referenced study was validated at a load disturbance ΔP=0.02pu with a settling time band determined at ±0.05, whereas in the proposed method, the load disturbance is ΔP=0.08pu with a settling time band at ±0.02. Despite this, the overshoot in our approach (0.019%) is superior to the overshoot in reference [33] (1.34%).

Table I

Comparison between previous and proposed work

Ref.	Year	Control Method	ΔP (pu)	Cont. tech.	Δf (Hz)			
					T_s (Sec)	M_P (%)	T_P (Sec)	U_P (%)
[20]	2017	PI-Observer	0.01		8	0.1	1.5	-0.06
		Luenberger Observer	0.01	LFC	8	0.1	1.5	-0.05
[21]		GA-PID	0.01		4.29	0.045	3	-1.5
		GA-PID	0.02	LFC+AVR	13.986	0.079	4.5	-3.2
	2022	GWO-PID	0.05		15.294	0.162	7.5	-11.1
[22]	2019	NLTA-PID	0.02	AVR+LFC	0.74	1.34	0.23	NA
[29]	2023	FPIDD^2	0.01	LFC	13.8	0.003	5.5	-0.018
[30]	2022	PID			20.33	0.0014	10	- 0.005
		Classical. V .rot	0.02		16.4	0.0012	9.5	- 0.005
		Adap. V .rot		LFC	14.6	0.001	9	- 0.004
		PID			86.332	0.00	-	- 0.006
		Classical. V .rot	0.1		67.2850	0.003	12	- 0.006
		Adap. V .rot			57.452	0.0018	7	- 0.006
[31]	2017	PI-LFC			18	0.0002	3.5	-0.0028
		LMI-LFC	0.01	LFC	25	0.002	10	-0.0029
		LMI-NPLFC			15	0.001	7	-0.0029
		LMI-PLFC			13	0.0002	7	-0.0024
Proposed control	2023	OFSTPID	0.08	LFC + AVR	3.16	0.019	0.572	-0.005

VI. Conclusion

In the submitted paper, a new approach was employed to study the control of Active Power Factor (APF) and Reactive Power Factor (RPF) in a turbogenerator system, based on concepts from real power system analysis using an OFSTPID controller. Conventional Load Frequency Control (LFC) was utilized to restore frequency due to active power variation, irrespective of changes in RPF with APF. The authors addressed the effects of desired active power generation on the reactive power generation in the turbogenerator system. Mathematical analysis of the real power system proposed demonstrated that as active power increases, reactive power decreases, and vice versa. This aligns with simulation results of conventional LFC based on PID controller, showing that when active power increased from 0.8pu to 0.88pu (10%), reactive power decreased from 0.6pu to 0.525pu (12.5%), and vice versa. This implies a proportional decrease in reactive power at loads, impacting load efficiency and performance. The OFSTPID controller was applied to the outer and inner loops of active and reactive power generation, aided by gain controllers ($G\_1, G\_2, G\_3, and\ G\_4$). The proposed control method's performance was verified to meet APF and deregulate the RPF of the turbogenerator system. Additionally, the power angle in the case of FSTPID (50.70) was smaller than in the case of LFC (53.220) at the same load requirements (±5% for increasing/decreasing APF), indicating the synchronous generator's ability to deliver larger active power with the proposed method. The results of this methodology were compared to other control methods for frequency deviation dynamic response.

References

[1] M. Nazari-Heris, S. Asadi, B. Mohammadi-Ivatloo, M. Abdar, H. Jebelli, and M. Sadat-Mohammadi, *Application of Machine Learning and Deep Learning Methods to Power System Problems*. Springer, 2022.

[2] A. E. Salem, S. H. Arafah, and O. M. Salim, "Power quality enhancement of grid-islanded parallel microsources using new optimized cascaded level control scheme," *Int. J. Electr. Power Energy Syst.*, vol. 140, p. 108063, 2022.

[3] A. E. Salem, S. H. Arafah, and O. M. Salim, "Power quality enhancement of grid-islanded parallel microsources using new optimized cascaded level control scheme," *Int. J. Electr. Power Energy Syst.*, vol. 140, no. September 2021, p. 108063, 2022, doi: 10.1016/j.ijepes.2022.108063.

[4] H. A. Yousef, A.-K. Khalfan, M. H. Albadi, and N. Hosseinzadeh, "Load frequency control of a multi-area power system: An adaptive fuzzy logic approach," *IEEE Trans. power Syst.*, vol. 29, no. 4, pp. 1822–1830, 2014.

[5] C. Mu, Y. Tang, and H. He, "Improved sliding mode design for load frequency control of power system integrated an adaptive learning strategy," *IEEE Trans. Ind. Electron.*, vol. 64, no. 8, pp. 6742–6751, 2017.

[6] S. K. Pandey, S. R. Mohanty, and N. Kishor, "A literature survey on load–frequency control for conventional and distribution generation power systems," *Renew. Sustain. Energy Rev.*, vol. 25, pp. 318–334, 2013.

[7] X.-C. Shangguan *et al.*, "Robust load frequency control for power system considering transmission delay and sampling period," *IEEE Trans. Ind. Informatics*, vol. 17, no. 8, pp. 5292–5303, 2020.

[8] M. Shiroei and A. M. Ranjbar, "Supervisory predictive control of power system load frequency control," *Int. J. Electr. Power Energy Syst.*, vol. 61, pp. 70–80, 2014.

[9] A. Sikander and P. Thakur, "A new control design strategy for automatic voltage regulator in power system," *ISA Trans.*, vol. 100, pp. 235–243, 2020.

[10] L. Yin, C. Zhang, Y. Wang, F. Gao, J. Yu, and L. Cheng, "Emotional deep learning programming controller for automatic voltage control of power systems," *IEEE Access*, vol. 9, pp. 31880–31891,

2021.

[11] L. B. Prasad, H. O. Gupta, and B. Tyagi, "Application of policy iteration technique based adaptive optimal control design for automatic voltage regulator of power system," *Int. J. Electr. Power Energy Syst.*, vol. 63, pp. 940–949, 2014.

[12] C. H. N. S. Kalyan *et al.*, "Comparative Performance Assessment of Different Energy Storage Devices in Combined LFC and AVR Analysis of Multi-Area Power System," *Energies*, vol. 15, no. 2, p. 629, 2022.

[13] C. H. Kalyan and G. S. Rao, "Impact of communication time delays on combined LFC and AVR of a multi-area hybrid system with IPFC-RFBs coordinated control strategy," *Prot. Control Mod. Power Syst.*, vol. 6, no. 1, pp. 1–20, 2021.

[14] M. Bhuyan, D. Chandra Das, and A. Kumar Barik, "Combined voltage and frequency response in a solar thermal system with thermostatically controlled loads in an isolated hybrid microgrid scheme," *Int. J. Sustain. Energy*, pp. 1–24, 2022.

[15] D. Sharma, V. Kushwaha, K. Pandey, and N. Rani, "Intelligent AVR control of a single thermal area combined with LFC loop," in *Intelligent Communication, Control and Devices*, Springer, 2018, pp. 779–789.

[16] K. R. M. V. Chandrakala and S. Balamurugan, "Simulated annealing based optimal frequency and terminal voltage control of multi source multi area system," *Int. J. Electr. Power Energy Syst.*, vol. 78, pp. 823–829, 2016.

[17] D. K. Lal and A. K. Barisal, "Combined load frequency and terminal voltage control of power systems using moth flame optimization algorithm," *J. Electr. Syst. Inf. Technol.*, vol. 6, no. 1, pp. 1–24, 2019.

[18] M. Taghdisi and S. Balochian, "Maximum power point tracking of variable-speed wind turbines using self-tuning fuzzy PID," *Technol. Econ. Smart Grids Sustain. Energy*, vol. 5, no. 1, pp. 1–8, 2020.

[19] V. P. Singh, N. Kishor, and P. Samuel, "Improved load frequency control of power system using LMI based PID approach," *J. Franklin Inst.*, vol. 354, no. 15, pp. 6805–6830, 2017, doi: 10.1016/j.jfranklin.2017.08.031.

[20] A. A. Hussein, S. S. Salih, and Y. G. Ghasm, "Implementation of Proportional-Integral-Observer Techniques for Load Frequency Control of Power System," *Procedia Comput. Sci.*, vol. 109, pp. 754–762, 2017, doi: 10.1016/j.procs.2017.05.307.

[21] N. Paliwal, L. Srivastava, and M. Pandit, "Application of grey wolf optimization algorithm for load frequency control in multi-source single area power system," *Evol. Intell.*, vol. 15, no. 1, pp. 563–584, 2022, doi: 10.1007/s12065-020-00530-5.

[22] N. Nahas, M. Abouheaf, A. Sharaf, and W. Gueaieb, "A Self-Adjusting Adaptive AVR-LFC Scheme for Synchronous Generators," *IEEE Trans. Power Syst.*, vol. 34, no. 6, pp. 5073–5075, 2019, doi: 10.1109/TPWRS.2019.2920782.

[23] A. Zaporozhets and V. Artemchuk, *Systems, Decision and Control in Energy II*, vol. 346. 2021. [Online]. Available: http://link.springer.com/10.1007/978-3-030-69189-9

[24] J. R. Nayak, B. Shaw, S. Das, and B. K. Sahu, "Design of MI fuzzy PID controller optimized by Modified Group Hunting Search algorithm for interconnected power system," *Microsyst. Technol.*, vol. 24, no. 9, pp. 3615–3621, 2018, doi: 10.1007/s00542-018-3788-3.

[25] T. Dogruer and M. S. Can, "Design and robustness analysis of fuzzy PID controller for automatic voltage regulator system using genetic algorithm," *Trans. Inst. Meas. Control*, vol. 44, no. 9, pp. 1862–1873, 2022, doi: 10.1177/01423312211066758.

[26] H. Eldem and E. Ülker, "The application of ant colony optimization in the solution of 3D traveling salesman problem on a sphere," *Eng. Sci. Technol. an Int. J.*, vol. 20, no. 4, pp. 1242–1248, 2017, doi: 10.1016/j.jestch.2017.08.005.

[27] V. Kumarakrishnan, G. Vijayakumar, D. Boopathi, K. Jagatheesan, S. Saravanan, and B. Anand, *Frequency Regulation of Interconnected Power Generating System Using Ant Colony Optimization Technique Tuned PID Controller*, vol. 822. 2022. doi: 10.1007/978-981-16-7664-2_11.

[28] B. Dhanasekaran, S. Siddhan, and J. Kaliannan, "Ant colony optimization technique tuned controller for frequency regulation of single area nuclear power generating system," *Microprocess. Microsyst.*, vol. 73, p. 102953, 2020, doi: 10.1016/j.micpro.2019.102953.

[29] A. A. Hossam-Eldin, E. Negm, M. Ragab, and K. M. AboRas, "A maiden robust FPIDD2 regulator for frequency-voltage enhancement in a hybrid interconnected power system using Gradient-Based Optimizer," *Alexandria Eng. J.*, vol. 65, pp. 103–118, 2023, doi:

10.1016/j.aej.2022.10.029.

[30] H. Abubakr, J. C. Vasquez, T. Hassan Mohamed, and J. M. Guerrero, "The concept of direct adaptive control for improving voltage and frequency regulation loops in several power system applications," *Int. J. Electr. Power Energy Syst.*, vol. 140, no. February, p. 108068, 2022, doi: 10.1016/j.ijepes.2022.108068.

[31] P. Ojaghi and M. Rahmani, "LMI-Based Robust Predictive Load Frequency Control for Power Systems with Communication Delays," *IEEE Trans. Power Syst.*, vol. 32, no. 5, pp. 4091–4100, 2017, doi: 10.1109/TPWRS.2017.2654453.